ACS OMEGA

http://pubs.acs.org/journal/acsodf

Article

High-Performance Solar Steam Generator Using Low-Cost Biomass Waste Photothermal Material and Engineering of the Structure

Mahmoud Maleki, Farzaneh Arabpour Roghabadi,* and Seyed Mojtaba Sadrameli

Cite This: *ACS Omega* 2022, 7, 39895−39906

Read Online

ACCESS | Metrics & More | Article Recommendations | Supporting Information

ABSTRACT: In this work, high-performance, low-cost, environmentally friendly multilayered solar steam generation systems are fabricated by engineering the structure and using a biomass photothermal material. Remarkably, the biomass photothermal material is extracted from the pyrolysis waste of linseed (flax) grains. The introduced system desalinates water using solar energy as the renewable source of energy, and its light absorber is from the waste of a renewable source. The biomass waste powder possesses a mesoporous structure, providing high light absorption through photon scattering and its high surface area. Moreover, to harvest the incident light efficiently and manage the thermal energy generated, devices including light absorbers with cone and cubic configurations and different water manager layers are fabricated and compared to each other. To confirm the high performance of the introduced photothermal material, different systems comprising graphite, graphene oxide, and carbon nanotube light absorbers are also fabricated. Using a biomass light absorber combined with harvesting of the light in different directions (cone configuration), the system with a water evaporation rate of 1.59 kg/m^{2}h corresponding to an efficiency of 92.9% is achieved. Furthermore, by depositing a thin layer of the transparent thermal superinsulator silica aerogel on the light absorber layer, the generated heat is localized and the heat losses are prevented, leading to a 7.5% enhancement of the water evaporation rate of the biomass system. The eco-friendly biomass-based system shows no significant change in its performance through operation for 40 desalination cycles of Persian Gulf water.

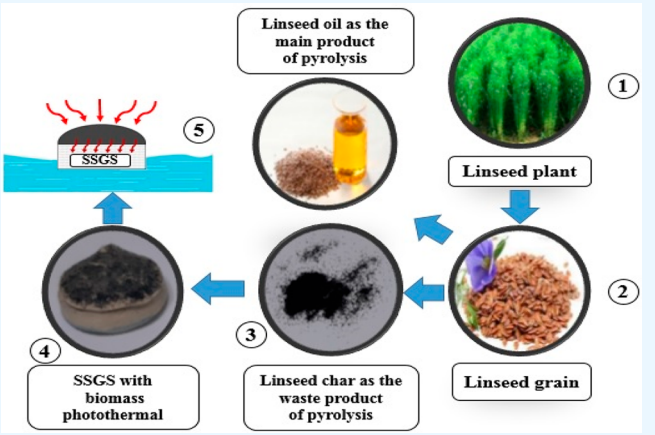

INTRODUCTION

Today, the shortage of drinking water is one of the main problems of societies that emphasizes the importance of the technologies used for water desalination. Recently, the limits and challenges caused by the consumption of fossil fuels have encouraged researchers to focus on technologies using solar energy for water desalination. Generally, solar energy as a free, clean, and abundant source of the energy can be employed for this purpose directly and indirectly.[1] In the indirect technology, solar energy is first converted into other forms of energy such as electrical energy using solar cells[2,3] and then utilized for water desalination. In contrast, in the direct method, the water is desalinated through the generation of steam in systems that absorb the solar photons.[4] The direct systems produce not only fresh water but also the steam generated by them that can be used for electricity generation.[5,6] One of the structures used for this technology is the floating configuration where the water is transferred controllably from the bulk to the device surface, and the evaporation occurs by consuming the heat generated from the photon energy absorption.[7,8] These systems should satisfy five important features including high light absorption, low thermal conductivity, efficient heat localization, easy and controllable water transfer, and the ability to float on the water surface.[9] In 2014, Ghasemi et al.[10] fabricated a bilayer solar steam generation system (SSGS) based on the graphite (G) absorber which can be considered as the initiation point for the study of these systems. Thus far, different systems have been studied that can be categorized into five groups regarding the utilized photothermal materials: graphene-based,[11−13] carbon-based,[5,6,14−19] wood- and biomass-based,[20−22] plasmonic and nanoparticle-based,[23−25] and polymer-based absorbers.[26−28] Interestingly, the aforementioned photothermal materials are employed as the absorber layer with different structures such as nanoparticles, porous particles or films, and thin films.[4] For instance, Cheng et al.[29] reported a reduced graphene oxide

Received: July 1, 2022
Accepted: October 6, 2022
Published: October 27, 2022

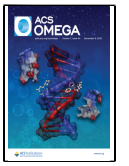

(rGO)-based solar absorption membrane that showed a water evaporation rate (WER) of 1.37 $kg{\cdot}m^{-2}{\cdot}h^{-1}$. Among the photothermal materials, biomass-based ones especially in the waste form not only are inexpensive candidates but also are eco-friendly materials with no destructive effect on the environment. Jiang et al.[14] fabricated high-performance SSGSs including light absorbers based on carbonized straw, rose, and coffee particles with micro-three-dimensional structures. They reported an efficiency of 93.4, 92.8, and 76% for the straw plants, roses, and coffee-based systems, respectively. In the same year, Wilson et al.[30] utilized porous carbon derived from the skin of lime (food waste) and a poly(vinyl alcohol) sponge for efficient steam generation and desalination of seawater. Their system produced steam with an efficiency of 90.88% and a WER of 1.386 $kg{\cdot}m^{-2}{\cdot}h^{-1}$ under one sun. Other forms of biomass such as green-tide waste,[31] carbonized loofah,[22] and green algae[32] have also been employed as the photothermal materials for this technology. Biomass-based carbonized particles possess three main advantages that have encouraged researchers to employ them as the photothermal materials: (1) wide particle size distribution that leads to the formation of a porous surface, (2) formation of a mesostructure that provides the absorption of most of the incident light through the scattering, and (3) the presence of pores and connected paths, providing the transfer of water and steam inside the structure. Pyrolysis waste is now a concern all over the world because of the entry of huge amounts of waste into nature that causes harmful effects on the environment. Different methods are employed to dispose of these wastes like burning, burying them in the ground, and releasing them into the water, resulting in irreparable damage to the environment. Therefore, reusing pyrolysis waste, especially for green applications such as the photothermal materials, can be beneficial for both the economy and the environment.

In addition to a suitable light absorber, other components of the device including the supports and water manager should satisfy the criteria needed for efficient SSGSs.[33] The heat generated in the system should be localized by preventing the conductive, convective, and radiative heat losses from the top and bottom sides of the systems. Polymeric foams have been introduced as promising candidates for the floating SSGSs because of their low density and thermal conductivity. In 2017, Shi et al.[34] built a two-layer SSGS with an absorber layer of graphene oxide (GO) and a sublayer of polystyrene (PS) foam, leading to an increase of the surface temperature of the system up to 10 °C on average compared to that in the system without PS foam. They reported a WER of 1.31 $kg{\cdot}m^{-2}{\cdot}h^{-1}$, equivalent to an efficiency of 83%. In another work, polyurethane (PU) foam was used as a suitable substrate with gold, silver, and GO photothermal materials, leading to an efficiency of 60% under one sun radiation.[35] Moreover, the system should transfer water controllably to balance the input energy and the steam generation rate. Cotton is one of the most important water transporters that has been utilized by many groups and researchers.[36,37] Inspired by the natural transpiration process in plants, Li et al.[38] designed a three-dimensional SSGS that resulted in better than 85% efficiency of steam production under one sun. In this system, a linen rod-shaped device was used to transfer water from the bulk to the surface of the system. Dao et al.[6] focused on the transpiration process of *Limnobium laevigatum* to build a system that generated fresh water and electricity simultaneously, which was based on multiwalled carbon nanotubes (MWNTs).

One of the challenges that these systems face is salt accumulation in the device components during the operation, which causes performance loss. Due to the imbalanced conditions that occur between the evaporation and water rising, salt can reach its crystallization concentration and deposit in pores and on the evaporation surface. Therefore, it is imperative to have sufficient water input when dealing with saline water and harsh conditions.[39] Therefore, practical and durable solutions are required to address these issues. Using photothermal materials with antifouling and salt-resistance properties or developing a device with a salt-rejection feature through the engineering of its structure is a feasible option.[40,41]

In addition to the type of the materials used for the layers of the system, the configuration also plays a key role in the process. Hong et al.[33] fabricated an engineered three-dimensional origami-based structure to absorb most of the incident light. Using GO and carbon nanotubes (CNTs) as the light absorbers, an extraordinary efficiency of nearly 100% was achieved. Various methods have been reported to engineer devices for drilling,[42,43] creating specific patterns,[44−46] making rod-shaped structures,[42,47] and creating a two-dimensional path.[48,49]

In this work, multilayered SSGSs are designed and fabricated. To achieve high-performance, low-cost, and eco-friendly devices, engineering the configuration, using biomass waste as the photothermal material, and localizing the generated heat are the focus. The low-cost photothermal material is extracted from the waste of the pyrolysis of linseed grains. To show the great potential of biomass waste as an alternative to the conventional photothermal materials, devices with graphene (G), GO, and CNTs are also fabricated. To harvest almost all of the incident light, the configuration of the light absorber layer is engineered using a cone structure, which is compared with the cubic one as a reference. For efficient heat localization through preventing heat losses, the device is covered by the synthesized transparent superinsulator silica aerogel layer. Moreover, different water manager types including felt, cellulose, and cotton fibers and various supports including open-cell PU foams, closed-cell PU foams, and PS foam are studied to make the best choice for preventing heat losses and evaporating water as much as possible. First, the morphology and structure of the used materials are studied by field emission scanning electron microscopy (FESEM), X-ray diffraction (XRD), Brunauer−Emmett−Teller (BET), and ultraviolet−visible (UV−vis) spectroscopy. Then the performance of the fabricated devices is investigated under the illumination of one sun. The water mass change during the illumination is measured and utilized to calculate the WER and efficiency.

MATERIALS AND METHODS

Materials. Closed-cell PU foam precursors, ISO370 resin, and Polymoc327/B2 curing agent were provided by Mokarar Company, Iran. Further, the open-cell PU foam precursors, HR 330 and ISO 8001G, were also supplied by Mokarar Company, Iran. G, GO, and CNTs were purchased from Sigma-Aldrich. Titanium dioxide was purchased from Evonik Industries AG (Germany). Tetraorthosilicate monomer (TEOS) and acetic acid as the precursors for silica aerogel (SiA) synthesis were supplied by Merck.

https://doi.org/10.1021/acsomega.2c04146
ACS Omega 2022, 7, 39895−39906

Table 1. Details of the Fabricated Multilayered SSGSs

		substrate		absorber layer composition			
sample name	configuration	insulator	water transfer layer		mg	dry density (g·cm^{-3})	wet density (g·cm^{-3})
Triple3 01	cubic	closed-cell PU	cotton fiber			0.160	0.496
Triple3 02	cubic	closed-cell PU	cotton fiber	G	240	0.162	0.505
				TiO_2	20		
				adhesive	400		
				water	7000		
Triple3 03	cubic	closed-cell PU	cotton fiber	GO	40	0.161	0.500
				adhesive	400		
				water	7000		
Triple3 04	cubic	closed-cell PU	cotton fiber	CNT	240	0.171	0.516
				TiO_2	20		
				adhesive	400		
				water	7000		
Triple3 05	cubic	closed-cell PU	cotton fiber	biomass	240	0.177	0.520
				TiO_2	20		
				adhesive	400		
				water	7000		
Triple6 01	cone	closed-cell PU	cotton fiber			0.152	0.479
Triple6 02	cone	closed-cell PU	cotton fiber	G	240	0.153	0.483
				TiO_2	20		
				adhesive	400		
				water	7000		
Triple6 03	cone	closed-cell PU	cotton fiber	GO	40	0.154	0.483
				adhesive	400		
				water	7000		
Triple6 04	cone	closed-cell PU	cotton fiber	CNT	240	0.161	0.490
				TiO_2	20		
				adhesive	400		
				water	7000		
Triple6 05	cone	closed-cell PU	cotton fiber	biomass	240	0.166	0.514
				TiO_2	20		
				adhesive	400		
				water	7000		

Synthesis of Silica Aerogels (SiA). Silica aerogel was synthesized by mixing 20 mL of TEOS with 128 mL of deionized (DI) water and stirred for 30 min. Then 45 mL of acetic acid was added to the prepared mixture and stirred. The mixture was poured into the mold and kept for 5 h to complete the gelation. The gels were immersed in DI water and kept at 60 °C for 12 h, followed by a solvent exchange process using propanol. Finally, the propanol solvent was removed from the gels through a supercritical drying step.

Preparation of Biomass Photothermal Material. As mentioned, the photothermal material introduced in this work was the waste of the pyrolysis of linseed grains without needing further complex processes. Typically, in the pyrolysis process in which its waste was used as the photothermal material in this work, the oil was first extracted by the cold pressing method followed by milling the grains to reduce the size. Then the fine grains smaller than 150 μm were separated and dried in an oven at 110 °C for 10 h. To pyrolyze the dried grains, a titanium−molybdenum reactor with a length of 45 cm and a diameter of 36 cm equipped with several control valves, thermocouples, barometers, condensers, and flares to burn indeterminate gases was used. Also, in order to supply the temperature and pressure of the reactor, a tube furnace and nitrogen gas were used. The residue of linseed was poured into the reactor. The nitrogen gas was then connected to the reactor inlet; the temperature was adjusted and the pyrolysis process was started. The duration of the pyrolysis reaction was between 1 and 1.5 h, and the heating rate was 20 °C·min^{-1}, where the final temperature was 530 °C. The output of the reactor was divided into three products: part I, gases burned by Feller; part II, the liquid coming out of the condenser as the main product of the pyrolysis that can be used for various applications such as a renewable fuel; part III, a black solid remains as the waste that is introduced as a low-cost and high-potential photothermal material in this work. In this work, this waste was collected and burned again at a temperature of 900 °C to remove impurities, and the desired biomass absorber was obtained. The schematic of the pyrolysis process is given in Figure S1.

Design and Fabrication of Solar Steam Generation Systems. In order to fabricate the multilayered systems, each layer was first prepared. The device support that also acted as the thermal insulator was selected among the three foams comprising open-cell PU foam, closed-cell PU foam, and PS foam. Closed- and open-cell PU foams were formed using mixtures of resin and curing agent. As an initial step, 10.4 g of ISO370 resin was sprayed onto the mold as a hydrophobic coating. Then 8 g of Polymoc327/B2 was added into the resin and immediately mixed at 1500 rpm for 30 s. Subsequently, the curing started, and after being shaped, the closed-cell PU foam

https://doi.org/10.1021/acsomega.2c04146
ACS Omega 2022, 7, 39895−39906

Table 2. Details of the Multilayered SSGSs Containing Silica Aerogel Thin Film

		substrate			thermal insulator	
sample name	structure	insulator	water transferring layer	absorber layer		mg
Triple6 05 + 5 g of Si	Triple6 05				SiA	5
Triple6 05 + 10 g of Si	Triple6 05				SiA	10
Triple6 05 + 20 g of Si	Triple6 05	closed-cell PU	cotton fiber	biomass	SiA	20
Triple6 05 + 40 g of Si	Triple6 05				SiA	40
Triple6 05 + 60 g of Si	Triple6 05				SiA	60

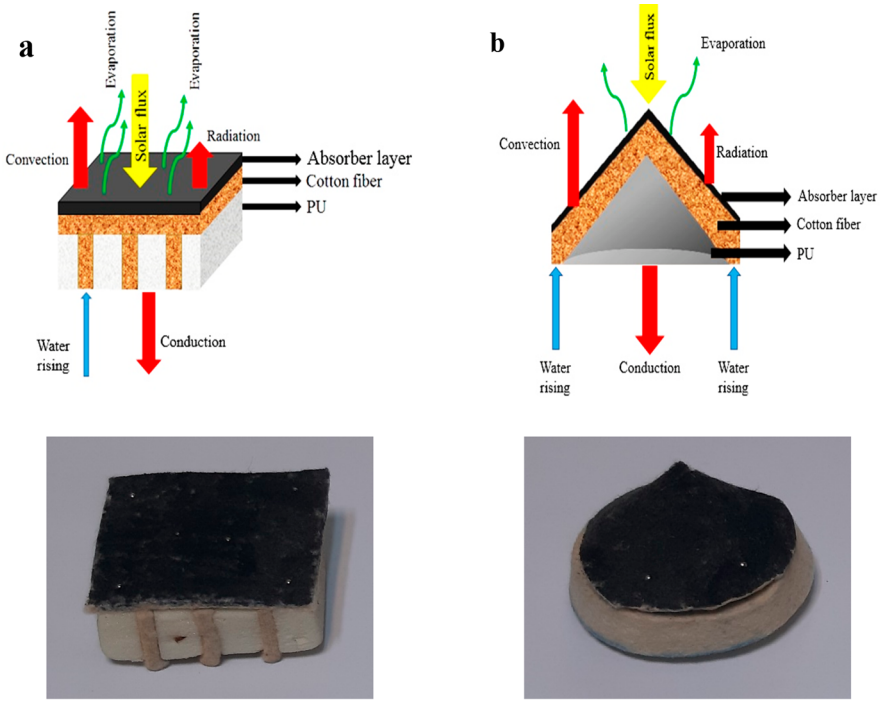

Figure 1. Schematic and photos of SSGSs with (a) cubic and (b) cone configurations.

was separated from the mold after 60 min. Similarly, open-cell PU foam was formed using 30 g of HR330 and 18 g of ISO 8001.

Different water transfer layers including 1.2 mm felt, 1.9 mm felt, cellulose, and cotton fibers were investigated to determine the best choice. First, the water transfer layer was washed with acetone and dried. To have a controllable water transfer process, the water transfer layer covered or was inserted into the PU foam with different configurations. The light absorber layer based on different photothermal materials was prepared using the compositions and configurations reported in Table 1. First, a mixture of the absorber (G, GO, CNT, biomass), titanium dioxide, polymeric acrylic adhesive, and deionized water was prepared and ultrasonicated for 15 min. As the next step, the cotton fiber layer was covered by the prepared mixture, followed by being dried in the oven at 110 °C for 20 min. Typically, in the SSGSs, the thickness of PU foam and felt layer was 2.5 and 0.31 cm, respectively. Regarding the absorber layer, since the density of the photothermal materials were different and also the felt surface was not uniform, it is estimated to be in the range of 500−600 μm (Figure S2).

The details of the samples containing silica aerogels as the transparent thermal insulator are summarized in Table 2. To form a thin film of the aerogels on the absorber, 5, 10, 20, 40, and 60 mg of silica aerogels was brushed on the absorber layer before being dried, leading to the formation of layers with different thicknesses.

Characterization. The morphology of the SSGS components was studied with a field emission scanning electron microscope (MIRA3TESCAN-XMU) and a LEICA DMLM optical microscope. The crystalline structure of the biomass was recorded by X-ray diffraction analysis (Rigaku Ultima IV). An Avantes UV−vis spectrophotometer is used to evaluate the optical properties of the photothermal materials. Furthermore, BET analysis (Belsro Mini II) was employed to investigate the porosity structure of the biomass-based photothermal material.

In order to evaluate the ability of the thermal insulators, the thermal conductivity of the layers (DECAGON company model KD2) was measured. A contact angle device (Jikan-CAG20) was utilized to evaluate the hydrophilicity of the different layers. Moreover, the mechanical strength of the support was evaluated via a universal testing machine (STM-20, Santam Co., Iran), where the compression and extension rates of the test were set at 20 and 10 mm·min^{-1}, respectively.

To investigate the performance of the fabricated systems, a sun simulator with a radiant power intensity of 100 mW·cm^{-2} (SHARIF SOLAR model SIM-10, Iran) was employed. The thermal profile of the systems illuminated by one sun was recorded by a thermographic camera (ThermoCam P200 OLIP). Also, to evaluate the performance of the systems in real conditions, the water samples were provided from the Persian

https://doi.org/10.1021/acsomega.2c04146
ACS Omega 2022, 7, 39895−39906

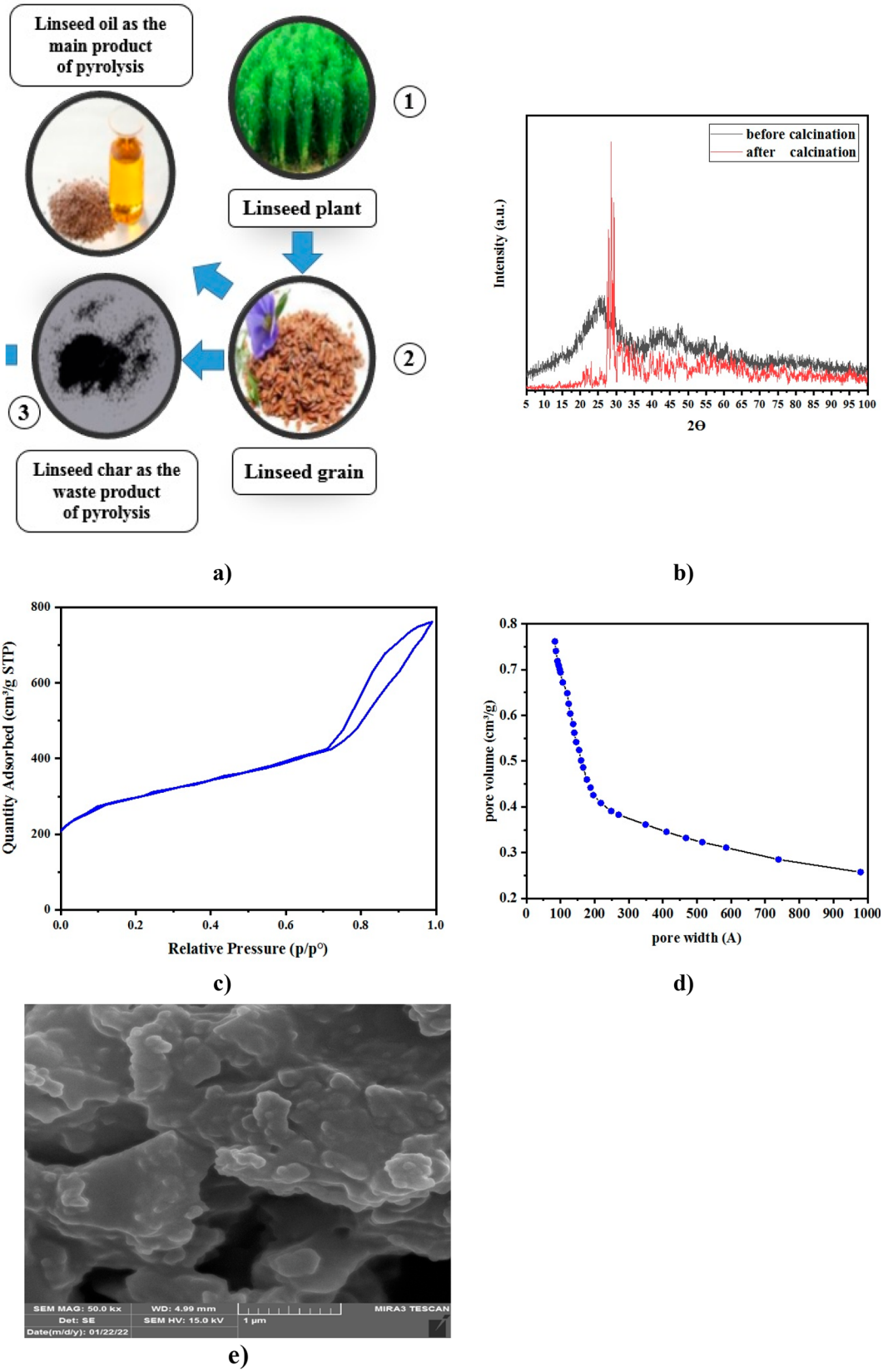

Figure 2. Biomass photothermal material (a) extracted from the waste of the linseed grain pyrolysis, (b) XRD, (c) BET curve of biomass photothermal material, (d) pore size distribution, and (e) FESEM image.

Gulf containing 4470 ppm of Na^+, 500 ppm Mg^{2+}, 160 ppm of Ca^{2+}, and 100 ppm K^+ ions. During the analysis, ambient temperature and relative humidity were maintained in the range of 24−26 °C and 30−35%, respectively. For measuring the performance, the water container covered by different SSGSs was illuminated by the sun simulator (one sun)

https://doi.org/10.1021/acsomega.2c04146
ACS Omega 2022, 7, 39895−39906

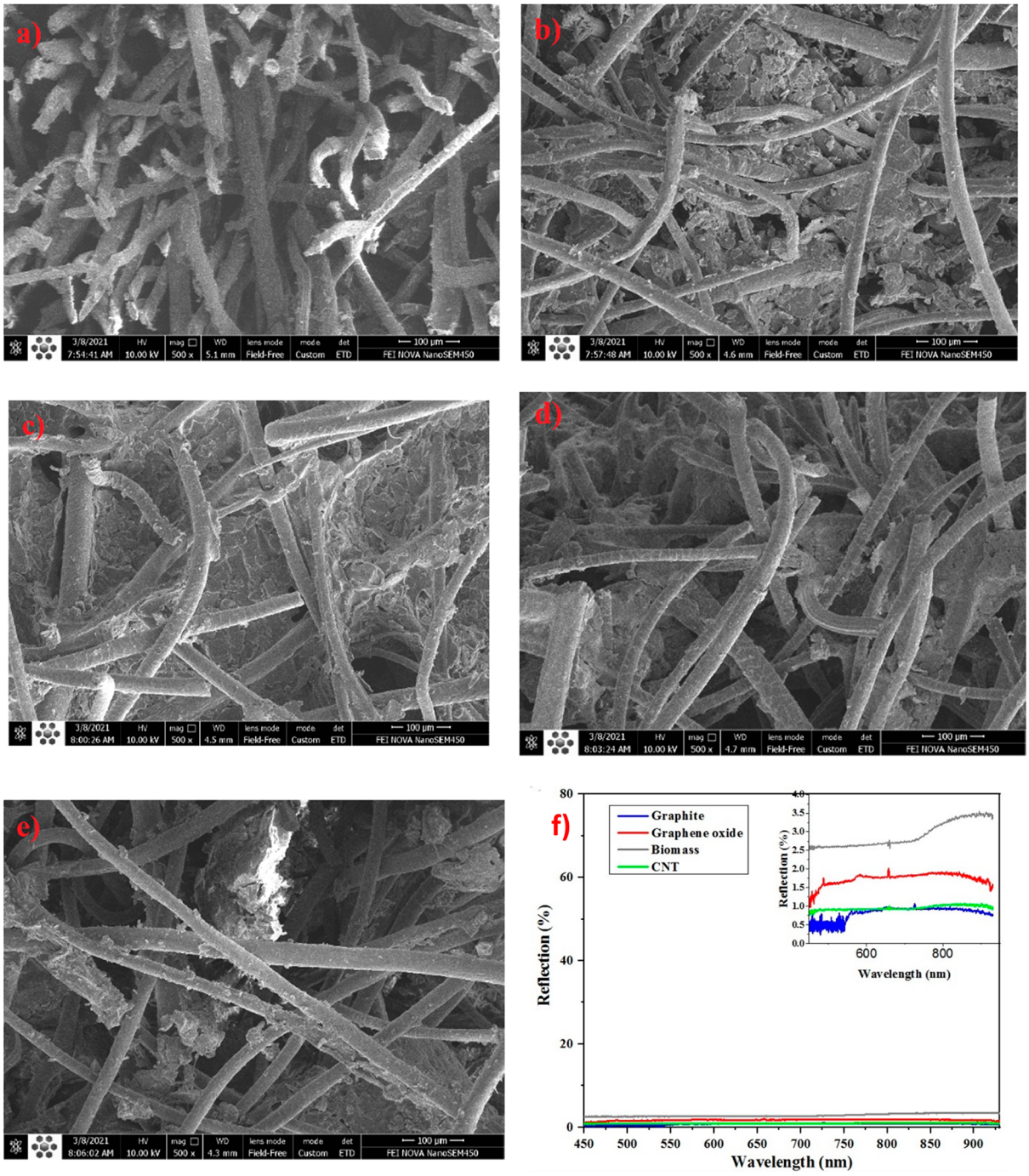

Figure 3. FESEM image of the surface of the SSGSs: (a) without absorber, (b) with G absorber, (c) with GO absorber, (d) with CNT absorber, (e) with biomass absorber, and (f) reflection spectra of different photothermal layers.

continuously. During the operation, the weight loss was recorded using a digital scale. Subsequently, the WER of the systems was measured using eq 1:

$$\text{evaporation rate} = \frac{m^{\circ}}{A} \tag{1}$$

where m° is the amount of water evaporated and A is the area of the light absorber. Moreover, eq 2 is used to determine the efficiency of light to heat conversion in SSGSs (η_{th}) (reused with permission from ref 10; copyright 2014 Springer Nature):

$$\eta_{th} = \frac{m^{\circ} h_{LV}}{C_{opt} q_i} \tag{2}$$

where h_{LV} is the total enthalpy of the liquid phase to vapor (sum of enthalpy of sensible heat and enthalpy of phase change), C_{opt} is the optical concentration, and q_i is the radiant power of the sun.

RESULTS AND DISCUSSION

As mentioned, in this work, photothermal material type, the configuration of the system, and heat localization by inserting

https://doi.org/10.1021/acsomega.2c04146
ACS Omega 2022, 7, 39895−39906

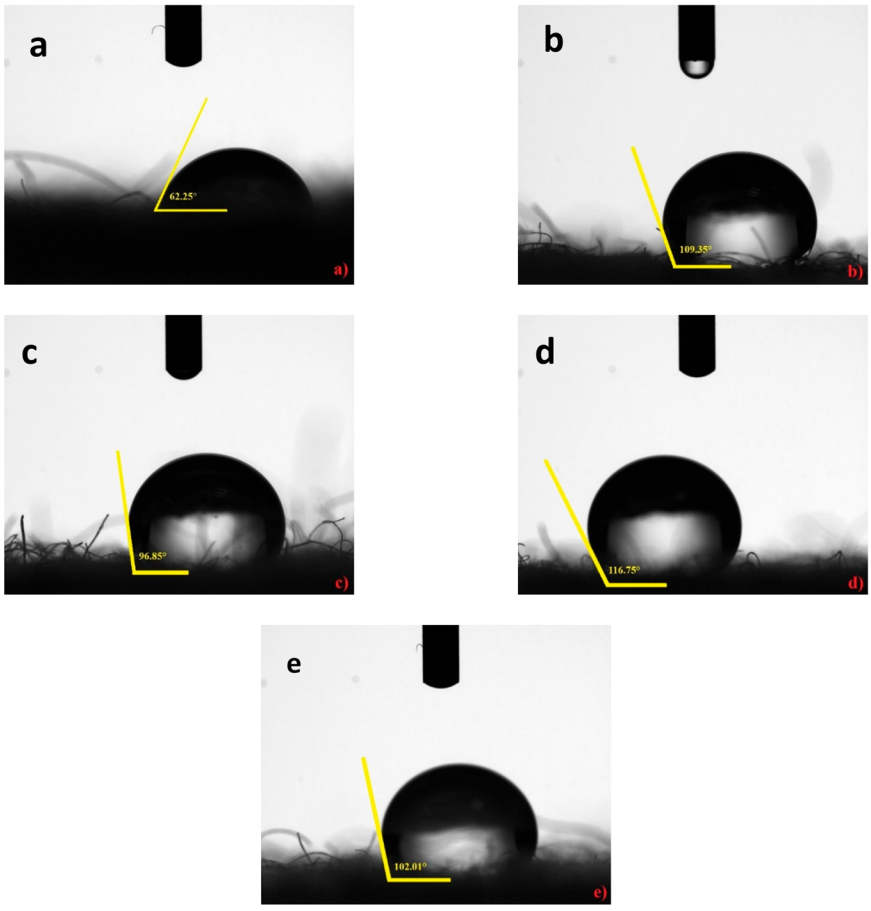

Figure 4. Contact angle of the surface of SSGSs: (a) without absorber, (b) with G absorber, (c) with GO absorber, (d) with CNT absorber, and (e) with biomass absorber.

an appropriate insulator are the focus to achieve highly efficient and low-cost SSGSs. Figure 1 and Figure S3 show the schematic diagram and the photos of the fabricated SSGSs with two configurations where harvesting more photons, transferring water more efficiently, and preventing heat losses are addressed. Since one of the main challenges in these systems is the heat losses due to conduction from the support to the bulk water, the thermal conductivity of the considered supports including open-cell and closed-cell PU foams in both dry and wet conditions is first measured (Table S1), which is also compared with the thermal conductivity of PS foam. According to these results, open-cell and closed-cell foams show conductive heat transfer coefficients of 0.052 and 0.037 $W{\cdot}m^{-1}{\cdot}K^{-1}$ in dry conditions and 0.104 and 0.039 $W{\cdot}m^{-1}{\cdot}K^{-1}$ in wet conditions, which are lower than the conductivity of PS foam. Achieving the higher conductivity in wet conditions is attributed to the presence of water that transfers heat more than does the PU foams. However, this difference is not significant for the closed-cell PU foam because the water is not allowed to enter cavities. Since the closed-cell PU foam is a better candidate to be used as the insulating substrate, all samples in this work are fabricated utilizing this one. The study of the mechanical properties of different substrates reveals that, among the three supports, the closed-cell PU foam with a compressive strength of 0.87 MPa is a promising candidate for this application (Figures S4−S8).

Since the closed-cell PU foam is hydrophobic, to transfer water from the bulk water to the surface, PU foam was covered by hydrophilic cotton fibers with two configurations presented in Figure 1. To have the best choice for a water transport layer, different types of hydrophilic layers including cotton fibers, 1.2 and 1.9 mm thick felts, and cellulose were first considered (Figures S9 and S10). According to the mechanical properties and water transferring rate of different layers, cotton fiber is the best candidate among the different types of layers investigated. It possesses a low heat transfer coefficient ($0.08\ W{\cdot}m^{-1}{\cdot}K^{-1}$) and transfers water from the bulk to the surface rapidly ($0.27\ mm{\cdot}s^{-1}$). As depicted in Figure S11, the surface of the system covered by cotton fibers is completely wet after 60 s. The cotton fibers show a tensile strength of 0.58 MPa (Figures S12−S15). Moreover, all systems with different configurations can float on the water surface (Figure S16).

As depicted in Figure 1, the surface of the PU foam is covered by cotton fibers that disperse water on the surface and act as the sublayer for depositing photothermal materials simultaneously. Figure 2 presents the morphological, structural, and crystalline properties of biomass photothermal material extracted from the pyrolysis waste of linseed grains. The XRD pattern of the biomass reveals that the biomass waste is an amorphous material before calcination, whereas the crystalline planes appear after it is calcinated at 900 °C. The BET diagram analysis (Figure 2c) indicates that the biomass powder has a surface area of 720.325 $m^2{\cdot}g^{-1}$ and a total porosity surface of 420.251 $m^2{\cdot}g^{-1}$. Also, the hysteresis diagram of biomass powder shows that the cavities of the structure of this powder are generally cylindrical shaped. According to the

https://doi.org/10.1021/acsomega.2c04146
ACS Omega 2022, 7, 39895−39906

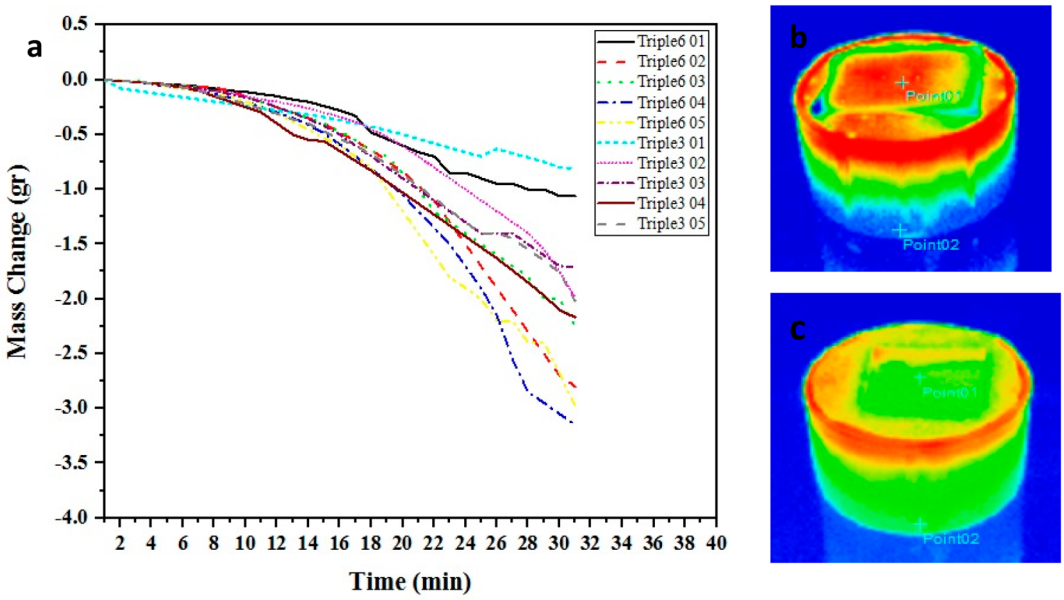

Figure 5. (a) Water mass change of the SSGSs, (b) thermography image of the water covered by biomass-based SSGSs, and (c) thermography image of the uncovered water.

structural results (Figure 2c–e), the biomass powder has a mesoporous structure with a porosity percentage of 92.6% that can be used as a suitable material for this application.

The FESEM images of the top surface of the SSGSs containing G, GO, CNTs, and a biomass absorber are presented in Figure 3. As can be seen, all of the absorbers are well-distributed on the surface of the system without blocking the pores, which are needed for water and steam transfer. Remarkably, the light reflection of all photothermal layers is less than 3.5%, indicating the harvesting of almost all incident photons (more than 97%) (Figure 3f). Moreover, as depicted in Figure S17, similar to the other photothermal materials used in this work, the biomass is a good absorber for almost all photons in the wavelength range of 300–900 nm.

Since the deposition of the light absorber on the cotton fibers changes its hydrophilicity, the surface properties are investigated by measuring the contact angle of the layers. The cotton fiber layer has a hydrophilic nature with a contact angle of 62.25° (Figure 4a). The addition of various absorbers reduces the hydrophilicity of the systems, whereas in the presence of G, GO, CNT, and biomass absorbers, the contact angles of 109.35, 96.85, 116.65, and 102.01° are achieved (Figure 4).

To evaluate the performance of the systems, they were illuminated under a sun simulator for 30 min in the same conditions. Figure 5a shows a graph of water mass changes during the operation of different SSGSs. The cone system with G (Triple6 02), GO (Triple6 03), CNT (Triple6 04), and biomass (Triple6 05) photothermal materials evaporates with 2.8, 2.25, 3.15, and 2.98 g of water, respectively. This value for the cubic system with G (Triple3 02), GO (Triple3 03), CNT (Triple3 04), and biomass (Triple3 05) photothermal materials is 1.99, 1.71, 2.17, and 2.02 g, respectively. Figure 5b,c shows the temperature distribution profile in the water that is covered by the biomass-based SSGS and the uncovered water, indicating the good heat localization in the presence of the SSGSs.

WER and energy conversion efficiency for the various SSGSs are shown in Figure 6. The results indicate that all studied

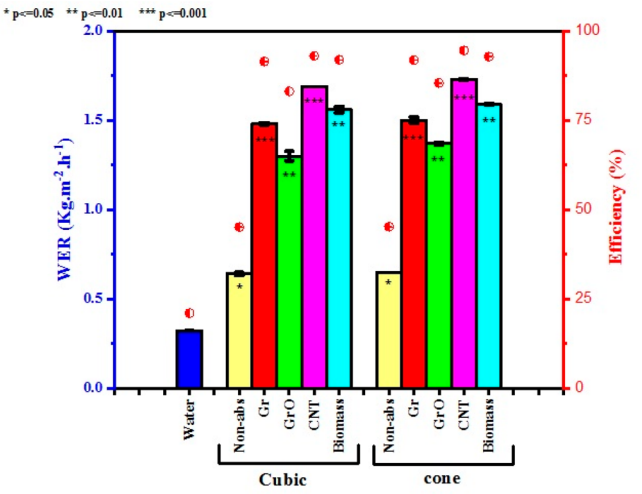

Figure 6. WER and efficiency of the fabricated SSGSs.

SSGSs possess a WER higher than that of the uncovered water, showing the superiority of these systems in the ability to produce steam and freshwater using solar energy. The devices with a cone configuration, G (Triple6 02), GO (Triple6 03), CNT (Triple6 04), and biomass (Triple6 05), show a WER of 1.5, 1.37, 1.73, and 1.59 $kg{\cdot}m^{-2}{\cdot}h^{-1}$, corresponding to an efficiency of 91.9, 85.5, 94.6, and 92.9%, respectively. In the G (Triple3 02), GO (Triple3 03), CNT (Triple3 04), and biomass (Triple3 05) devices with cubic configuration, the WER values of 1.48, 1.30, 1.69, and 1.56 $kg{\cdot}m^{-2}{\cdot}h^{-1}$ are achieved that are equivalent to an efficiency of 91.5, 83.2, 93.08, and 92%, respectively. The WER of uncovered water is only 0.32 $kg{\cdot}m^{-2}{\cdot}h^{-1}$, which is equivalent to a 21% efficiency. As a result, the performance of the systems with a cone configuration is slightly higher than the performance of the cubic one. For example, a comparison of two Triple6 04 and

https://doi.org/10.1021/acsomega.2c04146
ACS Omega 2022, 7, 39895–39906

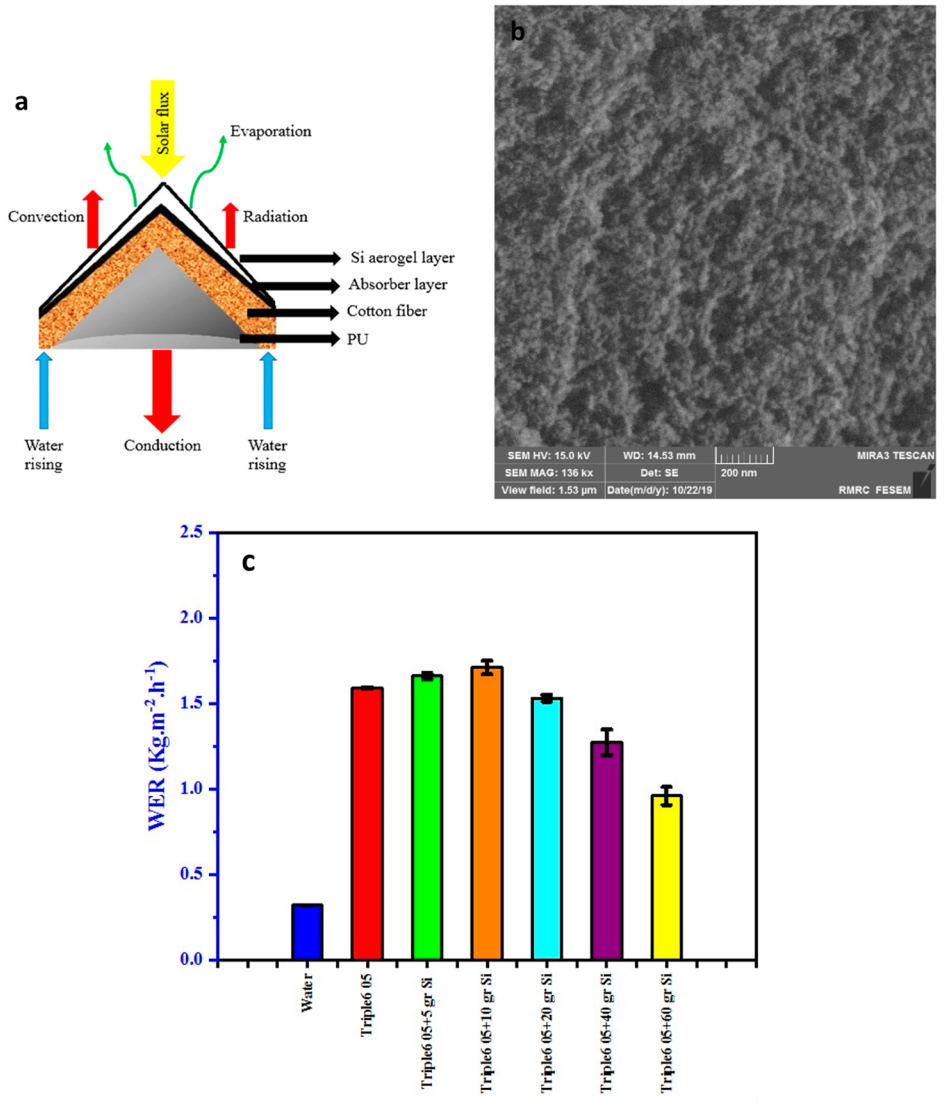

Figure 7. (a) Schematic of the SSGS covered by hydrophilic silica aerogel layer, (b) FESEM image of silica aerogels, and (c) WER of the cone SSGSs with biomass absorber and different amounts of hydrophilic silica aerogel.

Triple3 04 systems with the same photothermal layer but different configurations depicts that the WER of the system with a cone geometry is 8% higher than that of the cubic one. Since the cone systems can absorb light in different directions, harvesting more light and subsequently generating more heat in the cone systems is the main reason for achieving higher efficiency. It should be noted that the area of the absorber layer in the system with a cone configuration is higher than that of the cubic one. Thus, there is a competition between the bigger area and absorbing more photons from different angles, where the photon harvesting is dominant though its effect is not significant.

According to the results of the systems with different photothermal materials, the introduced biomass waste is a promising candidate since it shows a high performance in the range of the performance of the systems based on the conventional light absorbers. Moreover, the biomass photothermal material is low-cost and compatible with the environment as it is extracted from the waste of the pyrolysis process of linseed grains, which can be considered as a renewable source.

In order to prevent radiation and convection heat losses from the surface of the systems, a thin layer of the superinsulator hydrophilic silica aerogel was added on the surface of the biomass system (Figure 7a). The transparent silica aerogels possess a mesoporous structure (Figure 7b), where the BET surface area and total porosity surface are found to be 880.2877 and 543.203 m^2/g with a porosity percentage of 92.61%. The silica aerogels' hysteresis curve indicates the cylindrical shaped cavities (Figure S18).

Different amounts of silica aerogels are deposited on the light absorber layer. As shown in Figure 7c, the use of a thin layer of silica aerogel on the biomass absorber (Triple6 05 + 10 g of Si) as the optimum level increases the WER of the biomass system from 1.59 $kg{\cdot}m^{-2}{\cdot}h^{-1}$ (Triple6 05) to 1.71 $kg{\cdot}m^{-2}{\cdot}h^{-1}$ (Triple6 05 + 10 g of Si). When the amount of superinsulator is greater than 10 g, the performance decreases. It can be attributed to the loss of the incident photons through multiscattering in the silica aerogel layer. Moreover, thicker superinsulator layers can act as the barrier for transferring the steam generated in the light absorber layer.

https://doi.org/10.1021/acsomega.2c04146
ACS Omega 2022, 7, 39895−39906

One of the most important challenges in the SSGSs is the stability of their performance during operation. In order to evaluate the stability of the studied systems, the performance of these systems is measured 40 times and each time for 30 min. As shown in Figure 8, the best system shows no significant

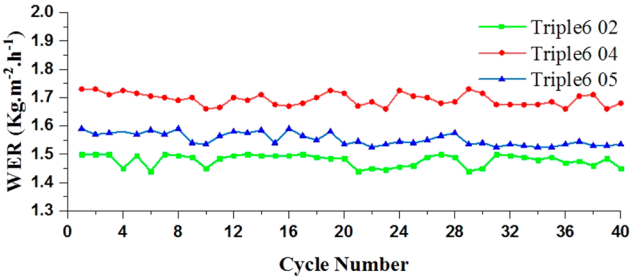

Figure 8. WER of the best systems for 40 cycles.

reduction in the WER after 40 repetitions, revealing the proper features of the components of the systems that prevent salt scaling and also the balanced water transfer.

As mentioned, the biomass absorber used in this work has not been studied before. To demonstrate its benefits, the following comparison between the WER and efficiency of this work and literature is made and summarized in Table 3, helping readers make qualitative judgments. However, the biocompatibility, low cost, and extraction from the biomass waste are the main advantages of the introduced biomass photothermal material that cannot be compared with other works.

CONCLUSION

As a summary, highly efficient, low-cost, and environmentally compatible SSGSs were fabricated by introducing a new biomass-based photothermal material and engineering of the structure. Remarkably, the source of the introduced biomass photothermal material was the waste of the pyrolysis process of linseed grains, providing significant environmental benefits. To achieve highly efficient devices, in addition to using desired photothermal material, engineering of the device configuration was also considered to harvest more light. Thus, devices with two configurations of cubic and cone shapes were fabricated. To signify the importance of the biomass light absorber and the level of its performance, different devices containing G, GO, and CNTs were also fabricated and compared in the cases of WER and efficiency. It was concluded that, among the two cubic and cone configurations, the last one provides better performance since it harvests more light from different angles. Surprisingly, the biomass absorber provided the device with a WER of 1.59 kg·m^{-2}·h^{-1} (efficiency of 92.9%), which was comparable to the WERs achieved for the devices containing G (1.5 kg·m^{-2}·h^{-1}), GO (1.37 kg·m^{-2}·h^{-1}), and CNTs (1.73 kg·m^{-2}·h^{-1}). Moreover, as another strategy to enhance the performance of the device, a thin layer of hydrophilic silica aerogel was used as the transparent superinsulator to prevent the heat losses from the top side of the systems. In this regard, the devices were covered by different amounts of silica aerogels. Using the optimum level of superinsulator, a 7.5% enhancement of WER was achieved by reducing the convective and radiative heat losses. Also, the results of stability test showed no significant reduction of WER after 40 times of using the system.

ASSOCIATED CONTENT

Supporting Information

The Supporting Information is available free of charge at https://pubs.acs.org/doi/10.1021/acsomega.2c04146.

Schematic of the pyrolysis process; images of prepared systems and their components; result analysis for compressive strength; result analysis for tensile strength; optical microscope images; self-floating test; absorbance spectra; BET curve (PDF)

AUTHOR INFORMATION

Corresponding Author

Farzaneh Arabpour Roghabadi − *Faculty of Chemical Engineering, Tarbiat Modares University, Tehran 1445703351, Iran; Optoelectronics and Nanophotonics Research Group, Faculty of Electrical and Computer Engineering, Tarbiat Modares University, Tehran 14115-111, Iran;* orcid.org/0000-0003-2856-680X; Email: arabpour@modares.ac.ir

Authors

Mahmoud Maleki − *Faculty of Chemical Engineering, Tarbiat Modares University, Tehran 1445703351, Iran;* orcid.org/0000-0003-4624-7175

Seyed Mojtaba Sadrameli − *Faculty of Chemical Engineering, Tarbiat Modares University, Tehran 1445703351, Iran; Department of Engineering, German University of Technology in Oman, Muscat 1816, Oman;* orcid.org/0000-0002-9732-7012

Complete contact information is available at: https://pubs.acs.org/10.1021/acsomega.2c04146

Notes

The authors declare no competing financial interest.

Table 3. Comparing Different Kinds of SSGSs in the Literature

author	absorber	water manager	insulator	absorption (%)	WER (kg·m^{-2}·h^{-1})	efficiency (%)	ref
Wang et al.	MoS_2 magnetic nanosheets	MoS_2 magnetic nanosheets		96	1	66.26	50
Li et al.	graphite	wood	wood	<95	1.15	80	51
Ma et al.	MOF-derived porous carbons	air laid paper	EPE foam	97	1.222	84.3	52
Miao et al.	CNT membrane	filter paper	aerogel		1.31	84.6	53
Kiriarachchi et al.	Au/Ag NPs	cotton fiber	cotton fiber		1.4	86.3	54
this work	carbon nanotube	cotton fiber	PU	99	1.73	94.6	this work
this work	biomass	cotton fiber	PU	97.5	1.59	92.9	this work

https://doi.org/10.1021/acsomega.2c04146
ACS Omega 2022, 7, 39895−39906

■ ACKNOWLEDGMENTS

The authors would like to acknowledge the research department of Tarbiat Modares University (research groups of phase change materials, Grant No. IG-39710).

■ REFERENCES

(1) Thirugnanasambandam, M.; Iniyan, S.; Goic, R. A review of solar thermal technologies. *Renew. Sustain. Energy Rev.* **2010**, *14*, 312−322.
(2) Arabpour Roghabadi, F.; et al. Stability progress of perovskite solar cells dependent on the crystalline structure: From 3D ABX 3 to 2D Ruddlesden-Popper perovskite absorbers. *J. Mater. Chem. A* **2019**, *7*, 5898−5933.
(3) Arabpour Roghabadi, F.; Kokabi, M.; Ahmadi, V.; Abaeiani, G. Quantum dots crosslinking as a new method for improving charge transport of polymer/quantum dots hybrid solar cells and fabricating solvent-resistant film. *Electrochim. Acta* **2016**, *222*, 881−887.
(4) Karami, S.; Arabpour Roghabadi, F.; Maleki, M.; Ahmadi, V.; Sadrameli, S. M. Materials and structures engineering of sun-light absorbers for efficient direct solar steam generation. *Sol. Energy* **2021**, *225*, 747−772.
(5) Dao, V.-D. An experimental exploration of generating electricity from nature-inspired hierarchical evaporator: The role of electrode materials. *Sci. Total Environ.* **2021**, *759*, 143490.
(6) Dao, V.-D.; Vu, N. H.; Choi, H.-S. All day Limnobium laevigatum inspired nanogenerator self-driven via water evaporation. *J. Power Sources* **2020**, *448*, 227388.
(7) Liu, C.; et al. High-Performance Large-Scale Solar Steam Generation with Nanolayers of Reusable Biomimetic Nanoparticles. *Adv. Sustain. Syst.* **2017**, *1*, 1600013.
(8) Loo, S.-L.; et al. Solar-Driven Freshwater Generation from Seawater and Atmospheric Moisture Enabled by a Hydrophilic Photothermal Foam. *ACS Appl. Mater. Interfaces* **2020**, *12*, 10307−10316.
(9) Ni, G.; Li, G.; Boriskina, S. V.; Li, H.; Yang, W.; Zhang, T.; Chen, G. Steam generation under one sun enabled by a floating structure with thermal concentration. *Nat. Energy* **2016**, *1*, 16126.
(10) Ghasemi, H.; et al. Solar steam generation by heat localization. *Nat. Commun.* **2014**, *5*, 4449.
(11) Kuzmenkov, D. M.; et al. Solar steam generation in fine dispersions of graphite particles. *Renew. Energy* **2020**, *161*, 265−277.
(12) Tian, J.; Huang, X.; Wu, W. Graphene-Based Stand-Alone Networks for Efficient Solar Steam Generation. *Ind. Eng. Chem. Res.* **2020**, *59*, 1135−1141.
(13) Meng, S.; et al. A bridge-arched and layer-structured hollow melamine foam/reduced graphene oxide composite with an enlarged evaporation area and superior thermal insulation for high-performance solar steam generation. *J. Mater. Chem. A* **2020**, *8*, 2701−2711.
(14) Jiang, H.; et al. Multi-3D hierarchical biomass-based carbon particles absorber for solar desalination and thermoelectric power generator. *J. Mater. Sci. Technol.* **2020**, *59*, 180−188.
(15) Qi, Q.; Wang, Y.; Wang, W.; Ding, X.; Yu, D. High-efficiency solar evaporator prepared by one-step carbon nanotubes loading on cotton fabric toward water purification. *Sci. Total Environ.* **2020**, *698*, 134136.
(16) Shi, L.; Wang, X.; Hu, Y.; He, Y.; Yan, Y. Bio-inspired Recyclable Carbon Interface for Solar Steam Generation. *J. Bionic Eng.* **2020**, *17*, 315−325.
(17) Sui, Y.; Hao, D.; Guo, Y.; Cai, Z.; Xu, B. A flowerlike sponge coated with carbon black nanoparticles for enhanced solar vapor generation. *J. Mater. Sci.* **2020**, *55*, 298−308.
(18) Hu, G.; et al. Salt-Resistant Carbon Nanotubes/Polyvinyl Alcohol Hybrid Gels with Tunable Water Transport for High-Efficiency and Long-Term Solar Steam Generation. *Energy Technol.* **2020**, *8*, 1900721.
(19) Karami, S.; Arabpour Roghabadi, F.; Pashaei Soorbaghi, F.; Ahmadi, V.; Sadrameli, S. M. Highly Efficient Solar Steam Generators Based on Multicore@Shell Nanostructured Aerogels of Carbon and Silica as the Light Absorber−Heat Insulator. *Sol. RRL* **2021**, *5*, 2100048.
(20) Ghafurian, M. M.; Niazmand, H.; Ebrahimnia-Bajestan, E.; Taylor, R. A. Wood surface treatment techniques for enhanced solar steam generation. *Renew. Energy* **2020**, *146*, 2308−2315.
(21) Tang, J.; et al. Realization of Low Latent Heat of a Solar Evaporator via Regulating the Water State in Wood Channels. *ACS Appl. Mater. Interfaces* **2020**, *12*, 18504−18511.
(22) Lu, Y.; Wang, X.; Fan, D.; Yang, H.; Xu, H.; Min, H.; Yang, X.; et al. Biomass derived Janus solar evaporator for synergic water evaporation and purification. *Sustain. Mater. Technol.* **2020**, *25*, No. e00180.
(23) Li, Z.; et al. Broadband-absorbing WO3-x nanorod-decorated wood evaporator for highly efficient solar-driven interfacial steam generation. *Sol. Energy Mater. Sol. Cells* **2020**, *205*, 110254.
(24) Zheng, Z.; et al. High-absorption solar steam device comprising Au@Bi2MoO6-CDs: Extraordinary desalination and electricity generation. *Nano Energy* **2020**, *68*, 104298.
(25) Shang, M.; et al. Full-Spectrum Solar-to-Heat Conversion Membrane with Interfacial Plasmonic Heating Ability for High-Efficiency Desalination of Seawater. *ACS Appl. Energy Mater.* **2018**, *1*, 56−61.
(26) He, J.; et al. High-Performance Salt-Rejecting and Cost-Effective Superhydrophilic Porous Monolithic Polymer Foam for Solar Steam Generation. *ACS Appl. Mater. Interfaces* **2020**, *12*, 16308−16318.
(27) Xiao, C.; et al. Ag/polypyrrole co-modified poly(ionic liquid)s hydrogels as efficient solar generators for desalination. *Mater. Today Energy* **2020**, *16*, 100417.
(28) Wang, F.; Su, Y.; Li, Y.; Wei, D.; Sun, H.; Zhu, Z.; Liang, W.; Li, A. Salt-Resistant Photothermal Materials Based on Monolithic Porous Ionic Polymers for Efficient Solar Steam Generation. *ACS Appl. Energy Mater.* **2020**, *3* (9), 8746−8754.
(29) Cheng, G.; Wang, X.; Liu, X.; He, Y.; Balakin, B. V. Enhanced interfacial solar steam generation with composite reduced graphene oxide membrane. *Sol. Energy* **2019**, *194*, 415−430.
(30) Wilson, H. M.; Ahirrao, D. J.; Raheman Ar, S.; Jha, N. Biomass-derived porous carbon for excellent low intensity solar steam generation and seawater desalination. *Sol. Energy Mater. Sol. Cells* **2020**, *215*, 110604.
(31) Zhu, M.; et al. Biomass Carbon Materials for Efficient Solar Steam Generation Prepared from Carbonized Enteromorpha Prolifera. *Energy Technol.* **2020**, *8*, 1901215.
(32) Li, J.; et al. Migration Crystallization Device Based on Biomass Photothermal Materials for Efficient Salt-Rejection Solar Steam Generation. *ACS Appl. Energy Mater.* **2020**, *3*, 3024−3032.
(33) Hong, S.; et al. Nature-Inspired, 3D Origami Solar Steam Generator toward Near Full Utilization of Solar Energy. *ACS Appl. Mater. Interfaces* **2018**, *10*, 28517−28524.
(34) Shi, L.; Wang, Y.; Zhang, L.; Wang, P. Rational design of a bi-layered reduced graphene oxide film on polystyrene foam for solar-driven interfacial water evaporation. *J. Mater. Chem. A* **2017**, *5*, 16212−16219.
(35) Awad, F. S.; Kiriarachchi, H. D.; Abouzeid, K. M.; Özgür, Ü.; El-Shall, M. S. Plasmonic Graphene Polyurethane Nanocomposites for Efficient Solar Water Desalination. *ACS Appl. Energy Mater.* **2018**, *1*, 976−985.
(36) Zhang, P.; et al. Three-dimensional water evaporation on a macroporous vertically aligned graphene pillar array under one sun. *J. Mater. Chem. A* **2018**, *6*, 15303−15309.
(37) Wu, X.; Gao, T.; Han, C.; Xu, J.; Owens, G.; Xu, H. A photothermal reservoir for highly efficient solar steam generation without bulk water. *Sci. Bull.* **2019**, *64* (21), 1625−1633.
(38) Li, X.; et al. Three-dimensional artificial transpiration for efficient solar waste-water treatment. *Natl. Sci. Rev.* **2018**, *5*, 70−77.
(39) Li, H.; Yan, Z.; Li, Y.; Hong, W. Latest development in salt removal from solar-driven interfacial saline water evaporators: Advanced strategies and challenges. *Water Res.* **2020**, *177*, 115770.

https://doi.org/10.1021/acsomega.2c04146
ACS Omega 2022, 7, 39895−39906

(40) Xu, K.; Wang, C.; Li, Z.; Wu, S.; Wang, J. Salt Mitigation Strategies of Solar-Driven Interfacial Desalination. *Adv. Funct. Mater.* **2021**, *31*, 2007855.
(41) Nawaz, F.; et al. Innovative salt-blocking technologies of photothermal materials in solar-driven interfacial desalination. *J. Mater. Chem. A* **2021**, *9*, 16233−16254.
(42) Li, Y.; et al. Graphene oxide-based evaporator with one-dimensional water transport enabling high-efficiency solar desalination. *Nano Energy* **2017**, *41*, 201−209.
(43) Zhou, L.; Tan, Y.; Ji, D.; Zhu, B.; Zhang, P.; Xu, J.; Gan, Q.; Yu, Z.; Zhu, J.; et al. Self-assembly of highly efficient, broadband plasmonic absorbers for solar steam generation. *Sci. Adv.* **2016**, *2*, No. e1501227.
(44) Bai, B.; et al. High-efficiency solar steam generation based on blue brick-graphene inverted cone evaporator. *Appl. Therm. Eng.* **2019**, *163*, 114379.
(45) Ni, F.; et al. Micro-/Macroscopically Synergetic Control of Switchable 2D/3D Photothermal Water Purification Enabled by Robust, Portable, and Cost-Effective Cellulose Papers. *ACS Appl. Mater. Interfaces* **2019**, *11*, 15498−15506.
(46) Ni, G.; et al. A salt-rejecting floating solar still for low-cost desalination. *Energy Environ. Sci.* **2018**, *11*, 1510−1519.
(47) Wang, Y.; et al. Wettable photothermal hollow fibers arrays for efficient solar-driven desalination under omnidirectional illumination without salt precipitation. *Mater. Today Energy* **2020**, *16*, 100391.
(48) Peng, G.; et al. High efficient solar evaporation by airing multifunctional textile. *Int. J. Heat Mass Transfer* **2020**, *147*, 118866.
(49) Zou, Y.; Chen, X.; Guo, W.; Liu, X.; Li, Y. Flexible and Robust Polyaniline Composites for Highly Efficient and Durable Solar Desalination. *ACS Appl. Energy Mater.* **2020**, *3*, 2634−2642.
(50) Wang, Q.; Qin, Y.; Jia, F.; Li, Y.; Song, S. Magnetic MoS2 nanosheets as recyclable solar-absorbers for high-performance solar steam generation. *Renew. Energy* **2021**, *163*, 146−153.
(51) Li, T.; et al. Scalable and Highly Efficient Mesoporous Wood-Based Solar Steam Generation Device: Localized Heat, Rapid Water Transport. *Adv. Funct. Mater.* **2018**, *28*, 1707134.
(52) Ma, S.; Qarony, W.; Hossain, M. I.; Yip, C. T.; Tsang, Y. H. Metal-organic framework derived porous carbon of light trapping structures for efficient solar steam generation. *Sol. Energy Mater. Sol. Cells* **2019**, *196*, 36−42.
(53) Miao, E.-D.; et al. Enhanced solar steam generation using carbon nanotube membrane distillation device with heat localization. *Appl. Therm. Eng.* **2019**, *149*, 1255−1264.
(54) Kiriarachchi, H. D.; et al. Plasmonic chemically modified cotton nanocomposite fibers for efficient solar water desalination and wastewater treatment. *Nanoscale* **2018**, *10*, 18531−18539.

https://doi.org/10.1021/acsomega.2c04146
ACS Omega 2022, 7, 39895−39906